AGU100 ADVANCING EARTH AND SPACE SCIENCE

Geophysical Research Letters

RESEARCH LETTER

10.1029/2018GL079710

Key Points:

- An eastern equatorial Pacific stable oxygen isotope depth profile shows a weak and deep thermocline during the Last Glacial Maximum
- Regional compilation of surface to subsurface dwelling foraminifera shows the thermocline was deep throughout the eastern equatorial Pacific

Supporting Information:

- Supporting Information S1
- Data Set S1

Correspondence to:
H. L. Ford,
h.ford@qmul.ac.uk

Citation:
Ford, H. L., McChesney, C. L., Hertzberg, J. E., & McManus, J. F. (2018). A deep eastern equatorial Pacific thermocline during the Last Glacial Maximum. *Geophysical Research Letters*, *45*. https://doi.org/10.1029/2018GL079710

Received 31 JAN 2018
Accepted 6 OCT 2018
Accepted article online 12 OCT 2018

A Deep Eastern Equatorial Pacific Thermocline During the Last Glacial Maximum

H. L. Ford[1,2], C. L. McChesney[1,3], J. E. Hertzberg[4,5], and J. F. McManus[1]

[1]Lamont-Doherty Earth Observatory, Columbia University, Palisades, NY, USA, [2]Now at School of Geography, Queen Mary University of London, London, UK, [3]Department of Geography, Texas A&M University, College Station, TX, USA, [4]Department of Oceanography, Texas A&M University, College Station, TX, USA, [5]Now at Department of Ocean, Earth and Atmospheric Sciences, Old Dominion University, Norfolk, VA, USA

Abstract The mean state and variability of the tropical Pacific is influenced by the depth of the thermocline. During the Last Glacial Maximum (~21,000 years ago), the zonal sea surface temperature gradient across the equatorial Pacific was reduced and productivity was generally lower than modern. To understand the thermocline depth's role in determining the Last Glacial Maximum tropical mean state, we reconstruct the upper ocean $\delta^{18}O$ profile from multiple species of planktic foraminifera. We synthesize existing records of surface and subsurface dwelling foraminifera to reconstruct the vertical $\delta^{18}O$ gradient throughout the eastern equatorial Pacific. We find the thermocline was deeper during the Last Glacial Maximum than the Holocene throughout the eastern equatorial Pacific region. The thermocline depth's role in the dynamic forcing of the cold tongue contributed to the reduced zonal SST gradient across the equatorial Pacific, decreased productivity, and presumably impacted El Niño-Southern Oscillation variability relative to the Holocene.

Plain Language Summary The eastern equatorial Pacific is cold and biologically rich because of a shallow thermocline. The thermocline is a subsurface ocean horizon where temperature rapidly decreases with depth. This shallow thermocline in the eastern equatorial Pacific is a key component of the ocean-atmospheric connection that characterizes the tropical Pacific and El Niño-Southern Oscillation. But how was the thermocline different in the past? Here we reconstructed the thermocline during the most recent ice age and found the thermocline was deeper than today. This deep thermocline contributed to the overall temperature pattern of the tropical Pacific, decreased the biological productivity and likely influenced the El Niño-Southern Oscillation.

1. Introduction

The thermocline is a vital component of the coupled ocean-atmospheric system that determines the mean state and variability of the tropical Pacific (Fiedler & Talley, 2006). The eastern equatorial Pacific (EEP; Figure 1) is characterized by a cold tongue and an Eastern Pacific Warm Pool (EPWP). The thermocline is shallow in the east; in the cold tongue, upwelling favorable winds bring cold, nutrient rich water to the surface, whereas in the EPWP the surface is warm and well stratified. The western equatorial Pacific has warm sea surface temperatures (SSTs) with a deep thermocline (Rebert et al., 1985). The cold eastern and the warm western equatorial Pacific create a strong zonal SST gradient that generates strong atmospheric circulation, which reinforces the zonal SST gradient and thermocline tilt (deep in the west, shallow in the east). Perturbations in the thermocline depth, zonal SST gradient, and atmospheric circulation generate El Niño-Southern Oscillation (ENSO) events (Guilyardi et al., 2009).

During the Last Glacial Maximum (LGM; 19,000 to 24,000 years ago), pCO_2 concentrations were lower than today and an ice sheet covered North America (Clark et al., 2009). SST reconstructions show the equatorial Pacific was cooler than modern and that the western and eastern warm pools responded primarily to pCO_2 radiative forcing, while the cold tongue responded to pCO_2 radiative forcing and dynamic forcing (Ford et al., 2015; Koutavas et al., 2002; Lea et al., 2000). As a consequence of this variable cooling pattern, the zonal SST gradient was likely reduced during the LGM relative to today. Proxy reconstructions suggest that productivity was likely reduced during the LGM (Costa et al., 2017) despite an upwelling strength that was similar to today (Loubere, 2000). Given the thermocline depth's role in determining the mean state of the tropical Pacific, how did the thermocline contribute to the SST and productivity patterns during the LGM?

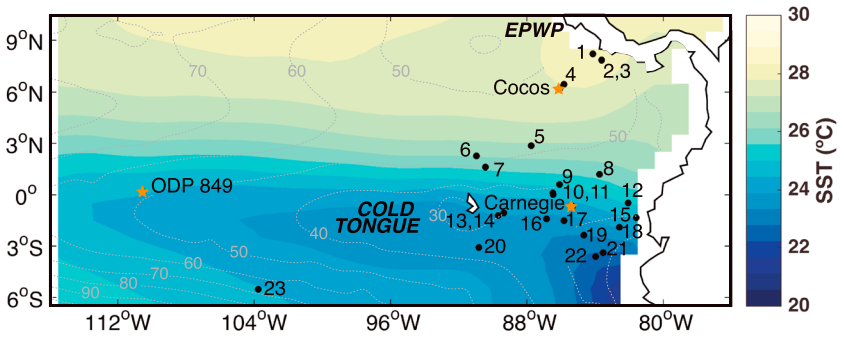

Figure 1. SST map with sites used in this study. Dashed contours are the 20 °C isotherm depth (meters) as a thermocline depth proxy. Stars are locations of new data and numbers are locations of published data (Table 2). ODP = Ocean Drilling Program; EPWP = Eastern Pacific Warm Pool; SST = sea surface temperature.

Limited faunal (Andreasen & Ravelo, 1997) and stable isotope (Loubere, 2001; Patrick & Thunell, 1997; Xu et al., 2010) records suggest the thermocline was deep during the LGM; however, there are few records that capture the spatial heterogeneity of the EEP (i.e., within the EPWP and cold tongue). Here we use stable isotopes of multiple species of planktic foraminifera to reconstruct upper water column profiles to infer changes in thermocline structure at Ocean Drilling Program (ODP) Site 849, located in the western extension of the cold tongue. We also synthesize existing and generate new $\delta^{18}O$ records of surface and subsurface dwelling foraminifera to (1) examine the surface and subsurface spatial $\delta^{18}O$ variability and (2) reconstruct the vertical $\delta^{18}O$ gradient as a thermocline depth proxy. We find the thermocline was deeper throughout the EEP region during the LGM relative to the Holocene.

2. Materials and Methods

2.1. Reconstructing the Thermocline Depth Profile

Holocene and LGM $\delta^{18}O$ depth profiles were created using six different species of planktic foraminifera at ODP Site 849 (Figure 1; 0°10.983′N, 110°31.183′W, 3,839 m water depth). We analyzed two sets of samples from the Holocene and LGM (n = 4 total; Table 1; age model: Ford et al., 2015; Mix et al., 1995). Approximately 10–60 specimens of *Globigerinoides ruber* (250–355 μm), *Trilobatus sacculifer* (*née Globigerinoides*, 355–425 μm), *Globorotalia menardii* (600–850 μm), *Pulleniatina obliquiloculata* (300–350 μm), *Neogloboquadrina dutertrei* (>350 μm), and *Globorotalia tumida* (355–425 μm) were picked. Samples were sonicated in deionized water and oven dried prior to analysis. Samples were run at the Stable Isotope Laboratory at Lamont-Doherty Earth Observatory of Columbia University on a Thermo Scientific Kiel IV Automated Carbonate Device coupled to a Thermo Scientific MAT 253 dual inlet isotope ratio mass spectrometer. The analytical uncertainty is 0.06‰ for $\delta^{18}O$ (NBS-19 standard).

For comparison to our Holocene and LGM $\delta^{18}O$ depth profiles, we used modern hydrographic data (Figure 2a) to calculate the predicted $\delta^{18}O$ of carbonate at Site 849 ($\delta^{18}O_{carbonate}$). $\delta^{18}O_{carbonate}$ is a function of temperature and the $\delta^{18}O$ of seawater ($\delta^{18}O_{seawater}$), which is related to salinity. To calculate $\delta^{18}O_{carbonate}$ (Figure 2b), we used average annual temperature (Locarnini et al., 2010), global gridded $\delta^{18}O_{seawater}$ data (Legrande & Schmidt, 2006), and the low-light paleotemperature equation of (Bemis et al., 1998). In the EEP, temperature determines the density structure of the upper ocean as salinity and $\delta^{18}O_{seawater}$ are largely invariant (Figure 2a). Thus, we argue the $\delta^{18}O_{carbonate}$ values of vertically distributed planktic foraminifera are a good proxy for thermocline structure and depth.

Additionally, to constrain planktic foraminifera calcification depth variability in our Holocene and LGM $\delta^{18}O$ depth profiles, we summarized modern planktic foraminifera preferred calcification depths for the EEP (Figure 2b). Planktic foraminifera abundance and vertical distribution are influenced by mixed layer depth, temperature, chlorophyll concentrations, and other factors that change seasonally to decadally (Ravelo & Fairbanks, 1992; Rebotim et al., 2016; Rincón-Martínez et al., 2011). These factors may also influence the export of foraminifera to depth and their incorporation into the marine sediment archive (Kawahata et al., 2002; Thunell et al., 1983; Venancio et al., 2017). To consider this variability, we

Geophysical Research Letters

10.1029/2018GL079710

Table 1
Species Specific Calcification Depth (Depth μ [m]) and Standard Deviation (Depth σ) Estimates Used in the Monte Carlo Simulation (Supporting Information) and δ18O Data Generated in this Study

Species	Depth μ (m)	Depth σ	849B 1H-1 5–8cm	849B 1H-1 15–18cm	$\delta^{18}O$ μ	$\delta^{18}O$ σ	Pooled σ = $\delta^{18}O$ σ and instrumental σ	849B 1H-1 67–70cm	849B 1H-1 74–80cm	$\delta^{18}O$ μ	$\delta^{18}O$ σ	Pooled σ = $\delta^{18}O$ σ and instrumental σ	
Globigerinoides ruber	14	10	−1.63	−1.39	−1.51	0.17	0.18	−0.16	0.02	−0.07	0.13	0.14	
Trilobatus sacculifer	29	14	−1.21	−1.37	−1.29	0.17	0.18	0.36	0.09	0.22	0.13	0.14	
Pulleniatina obliquiloculata	64	24	−0.32	−0.34	−0.33	0.11	0.12	0.93	0.64	0.79	0.20	0.20	
Globorotalia menardii	47	13	0.20	−0.62	−0.21	0.02	0.06	1.13	0.52	0.82	0.20	0.21	
Neogloboquadrina dutertrei	76	41	0.54	0.60	0.57	0.58	0.58	1.47	1.19	1.33	0.43	0.44	
Globorotalia tumida	106	57	0.69	0.52	0.60	0.05	0.08	1.73	1.15	1.44	0.20	0.20	
Globorotalia inflata	248	173	0.22	0.26	0.24	0.12	0.13	0.81	0.90	0.86	0.41	0.42	
			Cocos 0.5cm	Cocos 4.25cm	Cocos 7.5cm	$\delta^{18}O$ μ		Cocos 77cm	Cocos 84cm	Cocos 92cm	Cocos 99cm	Cocos 106cm	$\delta^{18}O$ μ
Globigerinoides ruber			−3.08	−2.51	−2.55	−2.71		−0.96	−0.93	−0.65	−0.94	−1.17	−0.93
Neogloboquadrina dutertrei			−0.24	−0.47	−0.70	−0.47		0.80	0.97	0.98	1.02	0.91	0.93
			Carnegie 0.5cm	Carnegie 6cm	Carnegie 10cm	$\delta^{18}O$ μ		Carnegie 295cm	Carnegie 320cm	$\delta^{18}O$ μ			
Globigerinoides ruber			−1.99	−1.59	−1.87	−1.82		−0.42	−0.50	−0.46			
Neogloboquadrina dutertrei			0.12	0.23	0.49	0.28		1.35	1.75	1.55			

Note. Ocean Drilling Program Site 849, Cocos Ridge, and Carnegie Ridge Holocene and Last Glacial Maximum multispecies $\delta^{18}O$ values and average ($\delta^{18}O$ μ). For Site 849, a pooled standard deviation (pooled σ = $\delta^{18}O$ σ and instrumental σ) was calculated by combining the standard deviation ($\delta^{18}O$ σ) and the analytical uncertainty in the $\delta^{18}O$ measurement (0.06‰).

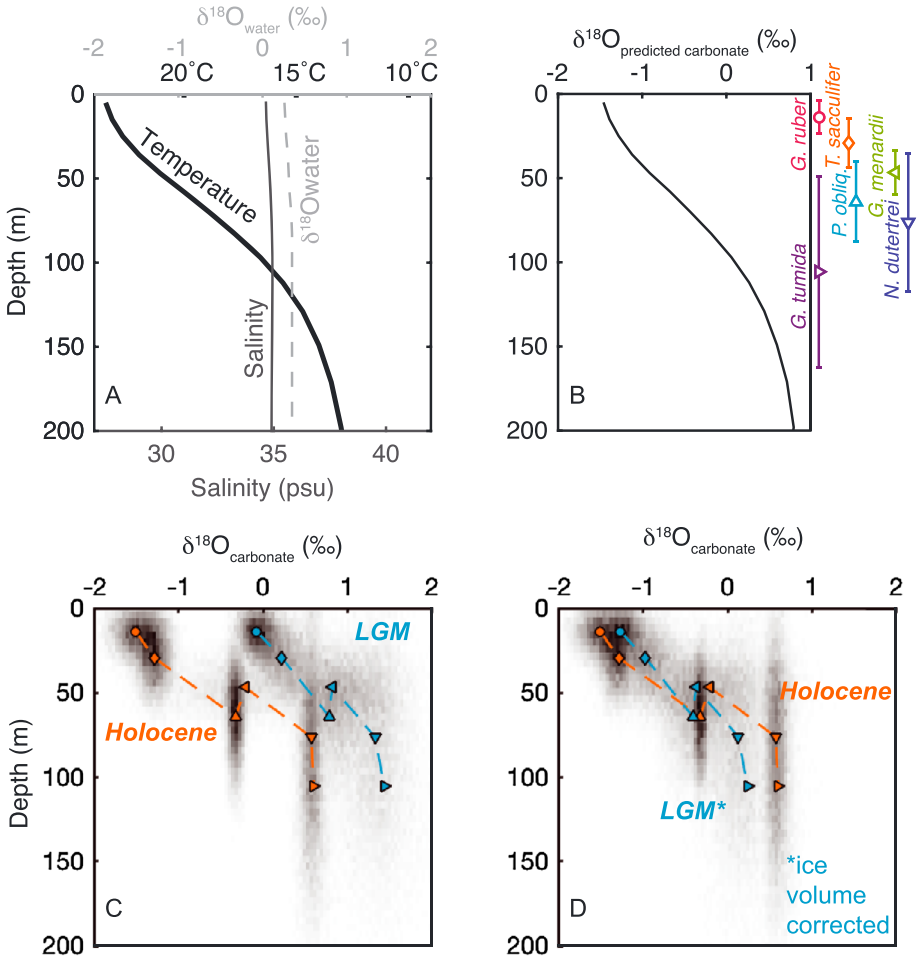

Figure 2. Multispecies $\delta^{18}O$ reconstruction at ODP Site 849. (a) Modern hydrography: temperature (black), salinity (gray), and $\delta^{18}O_{seawater}$ (Legrande & Schmidt, 2006; dashed gray). (b) Calculated $\delta^{18}O_{carbonate}$ and estimated foraminifera depths and standard deviations. (c) Average Holocene (orange) and LGM (blue) $\delta^{18}O$ profiles with Monte Carlo simulation histogram. (d) Same as in (c) but with LGM $\delta^{18}O$ values corrected for ice volume (~1.2‰; Fairbanks, 1989). LGM = Last Glacial Maximum.

summarized the available data from studies of the central to EEP to estimate a mean regional calcification depth and standard deviation (Figure 2a and Tables 1 and S1; Bé et al., 1985; Curry et al., 1983; Fairbanks et al., 1982; Faul et al., 2000; Loubere, 2001; Lynch-Stieglitz et al., 2015; Patrick & Thunell, 1997; Rincón-Martínez et al., 2011; Watkins et al., 1996). These studies represent a wide range of hydrographic conditions including the low productivity, deep thermocline EPWP, and high productivity, shallow thermocline cold tongue.

We then used a Monte Carlo simulation to estimate uncertainty in our planktic foraminifera $\delta^{18}O$ depth profiles related to calcification depth and $\delta^{18}O$ values (Table 1, Figure 2b). Using the planktic foraminifera (1) depth averages and standard deviation and (2) $\delta^{18}O$ averages and pooled standard deviation, we performed 10,000 Monte Carlo simulations (Figures 2c and 2d).

2.2. Thermocline Reconstruction Throughout the EEP

To reconstruct the surface and subsurface conditions across the EEP, we generated additional surface and subsurface dwelling foraminifera stable isotope data and used previously published records (Figure 1, Tables 1 and 2, and Data Set S1; Benway et al., 2006; Faul et al., 2000; Koutavas & Lynch-Stieglitz, 2003; Lea et al., 2000; Leduc et al., 2007, 2009; Lyle et al., 2002; Martínez et al., 2003; Patrick & Thunell, 1997; Pena

et al., 2008; Sadekov et al., 2013; Spero et al., 2003; Spero & Lea, 2002). Additional surface and subsurface dwelling foraminifera (Table 1, age model: Hertzberg et al., 2016) were analyzed at sites on the Cocos Ridge (MV1014-07MC: 6°14.037′N, 86°2.613′W, 1,995 m water depth and MV1014-08JC: 6°14.038′N, 86°2.613′W, 1,993 m water depth) and Carnegie Ridge (MV1014-09MC: 0°41.630′S, 85°19.995′W, 2,452 m water depth and MV1014-17JC: 0°10.832′S, 85°52.004′W, 2,867 m water depth) for the Holocene and LGM. Approximately 10–20 specimens of *G. ruber* (250–355 μm), and *N. dutertrei* (400–450 μm) were picked and sonicated in methanol prior to analysis. Samples were run at the Stable Isotope Geosciences Facility at Texas A&M University on a Thermo Scientific Kiel IV Automated Carbonate device coupled to a Thermo Scientific MAT 253 dual inlet isotope ratio mass spectrometer. The analytical uncertainty is 0.05‰ for $\delta^{18}O$ (NBS-19 standard).

Surface dwelling *G. ruber* and *T. sacculifer* and subsurface dwelling *N. dutertrei* and *G. tumida* $\delta^{18}O$ values were used to reconstruct mean Holocene (0–7,000 years) and LGM (19,000 to 24,000 years) conditions (Data Set S1). The available $\delta^{18}O$ values for a species were averaged within a time window (i.e., 0–7,000 years). If two species were available within a time window, they were then averaged together for a surface or subsurface mean. The mean Holocene value was then subtracted from the mean LGM value to calculate an anomaly. Note that 1.2‰ was subtracted from LGM values to correct for ice volume (Fairbanks, 1989). A LGM to Holocene subsurface to surface gradient was calculated by subtracting the surface mean from the subsurface mean. Here we use the subsurface to surface $\delta^{18}O$ gradient as a proxy for thermocline depth; this method has had wide applications outside the eastern Pacific (Fan et al., 2018; Nathan & Leckie, 2009; Sagawa et al., 2011), within the EEP (Jakob et al., 2017; Matsui et al., 2017; Patrick & Thunell, 1997; Ravelo & Shackleton, 1995; Spero et al., 2003), and is based on modern core-tops (Hollstein et al., 2017; Ravelo & Fairbanks, 1992; Venancio et al., 2017).

3. Results and Discussion

3.1. A Deep Thermocline at Site 849 During the LGM

The multispecies reconstruction at Site 849 indicates the thermocline strength was weaker and the thermocline depth was deeper during the LGM relative to the Holocene (Figure 2). During the Holocene, the vertical gradient between the surface and subsurface dwellers was ~2.0‰ whereas it was ~1.3‰ during the LGM. This reduced $\delta^{18}O$ vertical gradient during the LGM is consistent with a deeper thermocline. Ice volume-corrected LGM surface $\delta^{18}O$ values are lower and the subsurface $\delta^{18}O$ values (at the depth of *N. dutertrei* and *G. tumida*) are higher than the Holocene. Colder surface temperatures during the LGM compared to the Holocene are well documented in proxy reconstructions and modeling results (Otto-Bliesner et al., 2009). We predict isotopically lower than Holocene ice volume-corrected $\delta^{18}O$ values in the deeper thermocline during the LGM, but unfortunately our profile does not include deep-dwelling species such as *Globorotalia truncatulinoides* (absent from our samples) to verify this extrapolation. Accordingly, we suggest the LGM thermocline was thicker than the Holocene, resulting in an overall deepening of the thermocline.

3.2. Regional Patterns in Surface and Subsurface $\delta^{18}O$

Surface $\delta^{18}O$ values ($\delta^{18}O_{surface}$) from *G. ruber* and *T. sacculifer* show the EEP was generally cooler and/or characterized by heavy $\delta^{18}O_{seawater}$ values during the LGM in comparison to the Holocene (Figure 3a). The EPWP has the largest anomaly. The pattern within the cold tongue is more complex with heavier, equal to, or lighter $\delta^{18}O_{surface}$ values during the LGM in comparison to the Holocene. Overall, the meridional $\delta^{18}O_{surface}$ gradient across the EPWP and cold tongue was reduced (Koutavas & Lynch-Stieglitz, 2003). This is due in part to stronger cooling in the EPWP in comparison to the cold tongue during the LGM (Ford et al., 2015; Koutavas et al., 2002; although see Dubois et al., 2009, for a discussion of proxy choice). During the LGM, the EPWP primarily responds to pCO_2 radiative heating and its associated feedbacks (Ford et al., 2015). In contrast, the cold tongue responds to a variety of dynamic feedbacks during the LGM including a deep thermocline, weak winds, and a more southern position of the Intertropical Convergence Zone (Ford et al., 2015; Koutavas & Lynch-Stieglitz, 2003).

Subsurface $\delta^{18}O$ values ($\delta^{18}O_{subsurface}$) from *N. dutertrei* and *G. tumida* show the EPWP and cold tongue have different regional patterns (Figure 3b). From the LGM to the Holocene, the EPWP $\delta^{18}O_{subsurface}$ values decreased (an increase in temperatures and/or decrease in $\delta^{18}O_{seawater}$ values), whereas the cold tongue

Table 2
Site Locations

Site	Site number	Source	Lat. (°)	Long. (°)	Depth (m)
MD02-2529	1	Leduc et al., 2007; Leduc et al., 2009	8.2	−84.1	1,619
ODP1242	2	Benway et al., 2006	7.9	−83.6	1,364
ME0005A-43JC	3	Benway et al., 2006	7.9	−83.6	1,368
TR163-11	4	Martínez et al., 2003	6.5	−85.8	1,950
Cocos 07MC, 08JC	-	This study	6.2	−86.0	1,993
RC13-140	5	Koutavas & Lynch-Stieglitz, 2003	2.9	−87.8	2,246
TR163-19	6	Lea et al., 2000; Spero & Lea, 2002; Spero et al., 2003	2.3	−91.0	2,348
CD38-17P	7	Sadekov et al., 2013	1.6	−90.4	2,580
DSDP677B	8	Martínez et al., 2003	1.2	−83.7	3,473
DSDP506B	9	Martínez et al., 2003	0.6	−86.1	2,711
ODP849	-	This study	0.2	−110.5	3,839
Y69-71P	10	Lyle et al., 2002	0.1	−86.5	2,740
ODP1240	11	Pena et al., 2008	0.0	−86.5	2,921
V19-27	12	Koutavas & Lynch-Stieglitz, 2003	−0.5	−82.1	1,373
Carnegie 09MC, 17JC	-	This study	−0.7	−85.3	2,452
V21-29	13	Koutavas & Lynch-Stieglitz, 2003	−1.1	−89.4	712
V21-30	14	Koutavas & Lynch-Stieglitz, 2003	−1.2	−89.7	617
TR163-38	15	Martínez et al., 2003	−1.3	−81.6	2,200
RC8-102	16	Koutavas & Lynch-Stieglitz, 2003	−1.4	−86.9	2,180
RC11-238	17	Faul et al., 2000; Koutavas & Lynch-Stieglitz, 2003	−1.5	−85.8	2,573
TR163-33	18	Martínez et al., 2003	−1.9	−82.6	2,230
V19-28	19	Koutavas & Lynch-Stieglitz, 2003	−2.4	−84.7	2,720
ODP846B	20	Martínez et al., 2003	−3.1	−90.8	3,296
V19-30	21	Lyle et al., 2002	−3.4	−83.5	3,091
TR163-31	22	Patrick & Thunell, 1997	−3.6	−84.0	3,210
V21-40	23	Koutavas & Lynch-Stieglitz, 2003	−5.5	−103.8	3,182

$\delta^{18}O_{subsurface}$ values increased (a decrease in temperatures and/or an increase in $\delta^{18}O_{seawater}$ values). The limited subsurface records available do not show a consistent spatial pattern and suggest temperatures were 1–2 °C cooler or 1–2 °C warmer in the EEP (Ford et al., 2015; Hertzberg et al., 2016; Pena et al., 2008; Sadekov et al., 2013). The spatial subsurface temperature and $\delta^{18}O_{seawater}$ pattern within the EEP is currently poorly constrained.

3.3. A Deep Thermocline Throughout the EEP

Our synthesis of surface and subsurface $\delta^{18}O$ values shows, on average, the LGM subsurface to surface $\delta^{18}O$ gradient (Figure 3c) was reduced by 0.37‰ compared with the Holocene, suggesting the EEP thermocline was deeper during the LGM than the Holocene. This result is not sensitive to time interval choice within the Holocene (e.g., mid-Holocene [5,500 to 6,500 ka] vs. the last 7,000 years as used in this study). Planktic foraminifera calcification depth preferences are dependent on the coupled thermocline and nutricline in the tropical Pacific (Bé et al., 1985; Fairbanks et al., 1982; Faul et al., 2000; Patrick & Thunell, 1997; Rincón-Martínez et al., 2011; Watkins et al., 1996). If there was a change in calcification depth of the subsurface foraminifera used to calculate the subsurface to surface $\delta^{18}O$ gradient, this is likely a response to a change in thermocline/nutricline depth itself and thus integrated into the subsurface to surface $\delta^{18}O$ gradient calculation. The deep LGM EEP thermocline is corroborated by our multispecies $\delta^{18}O$ vertical depth Monte Carlo reconstruction at Site 849, the previously published $\delta^{18}O$ vertical profile at Site TR163-31B (Patrick & Thunell, 1997) and faunal reconstructions (Andreasen & Ravelo, 1997). As ocean and atmospheric dynamics are coupled in the EEP, a deep thermocline during the LGM has broad implications for productivity, upwelling, zonal SST reconstructions, and ENSO.

Costa et al. (2017) show the majority of productivity records ($^{231}Pa/^{230}Th$, excess Ba, opal, and organic carbon fluxes) indicate there was reduced productivity during the LGM, and we argue that the deep thermocline may have contributed to this low-productivity state. While the balance of productivity reconstructions suggest reduced productivity (Bradtmiller et al., 2006; Costa et al., 2016, 2017; Pichat et al., 2004), some show

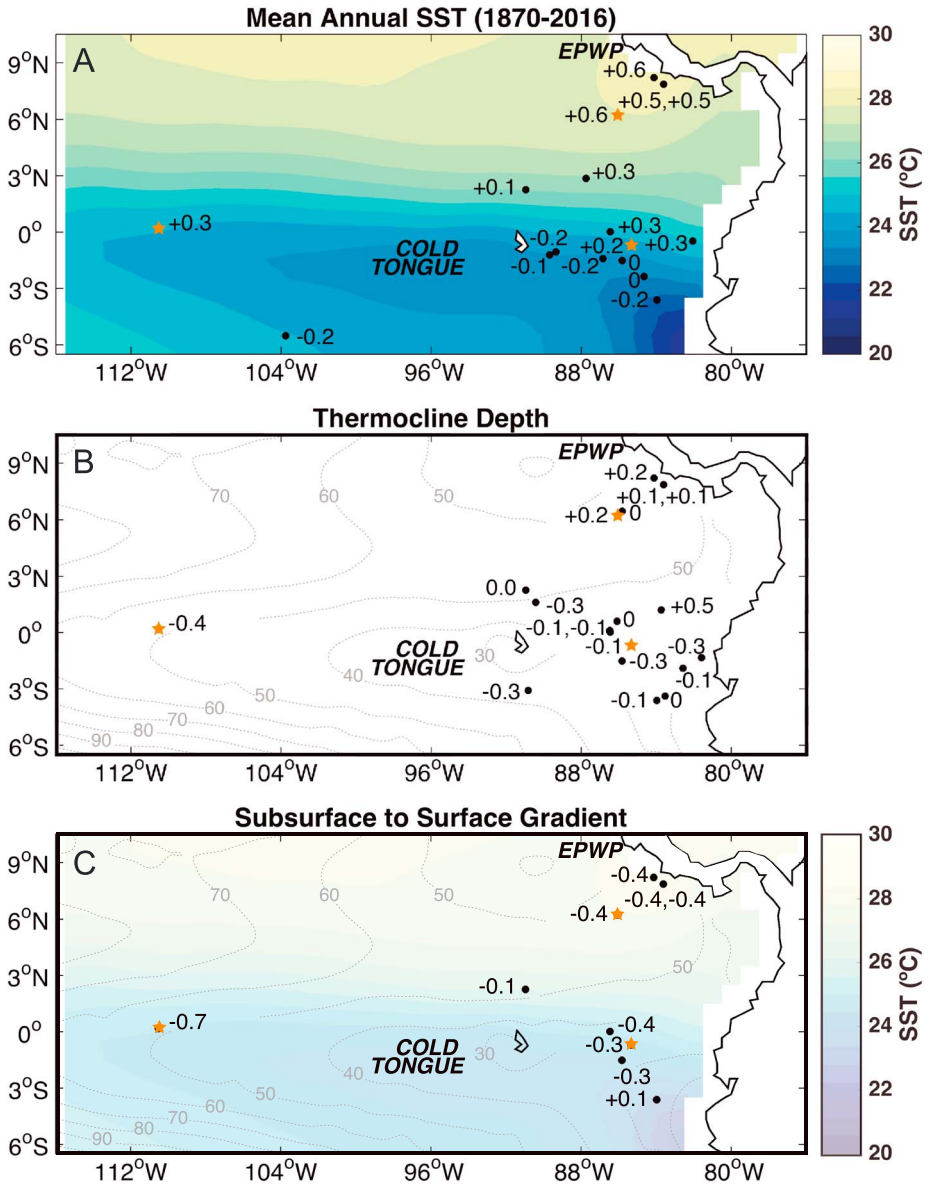

Figure 3. Synthesis of regional EEP $\delta^{18}O$ records. (a) LGM-Holocene (LGM minus Holocene) surface dwelling *G. ruber* and *T. sacculifer* $\delta^{18}O$ values overlain on a SST map. (b) LGM-Holocene subsurface dwelling *N. dutertrei* and *G. tumida* $\delta^{18}O$ values overlain on a 20 °C isotherm depth contour map (meters, dashed gray). (c) LGM-Holocene subsurface to surface $\delta^{18}O$ gradient overlain on a SST and 20 °C isotherm depth contour map. Stars indicate study locations where new data were generated. $\delta^{18}O$ values in ‰. EPWP = Eastern Pacific Warm Pool; SST = sea surface temperature; LGM = Last Glacial Maximum.

enhanced productivity (Lyle et al., 1988; Murray et al., 2012) during the LGM relative to today, likely related to the dynamic nature of the EEP and proxy interpretation. Although productivity is tightly linked to upwelling in the EEP today, upwelling has been relatively constant over the last 30,000 years (Costa et al., 2016; Loubere, 2000). This suggests changes in productivity are unrelated to changes in upwelling intensity and instead are related to thermocline depth, biological activity (Pichevin et al., 2009), nutrient availability (Rafter et al., 2012; Sarmiento et al., 2004), and/or dust fertilization (Costa et al., 2016; Loveley et al., 2017; Murray et al., 2012).

During the LGM, a deep thermocline may have contributed to the reduced productivity by limiting nutrient delivery to the surface via upwelling. In the modern ocean, upwelling-favorable winds exist across the

equatorial Pacific (Wyrtki, 1981); however, the western equatorial Pacific has low productivity because the thermocline is deep and the nutrients are beyond the vertical reach of Ekman pumping (Richards & Pollard, 1991). During the LGM, a deep thermocline within the cold tongue of the EEP may have limited nutrient delivery to the surface in a similar manner. Additionally, thermocline waters may have had lower nutrient concentrations and/or different sources during the LGM relative to modern (Costa et al., 2016; Loubere, 2001). Today, equatorial thermocline waters are sourced in the extratropics, mostly south Pacific midlatitude regions (Fiedler & Talley, 2006). An increase in the delivery of Southern Ocean intermediate waters (Pena et al., 2013), which were nutrient poor due to an increase in high-latitude nutrient utilization (Sarmiento et al., 2004), may have also limited productivity during the LGM.

The tropical SST pattern and a deep EEP thermocline suggest the LGM equatorial Pacific was in an El Niño-like mean state. Overall, the zonal SST gradient between the EEP cold tongue and western equatorial Pacific warm pool was reduced during the LGM (Ford et al., 2015; Koutavas et al., 2002). The EEP regional surface $\delta^{18}O$ (this study; Koutavas et al., 2002) and the balance of SST records indicate there was spatial heterogeneity in cooling during the LGM relative to modern. Surface temperatures in the EPWP and western equatorial Pacific warm pool were ~2.5 °C cooler during the LGM, whereas the EEP cold tongue was ~1.5 °C cooler (Benway et al., 2006; de Garidel-Thoron et al., 2007; Hertzberg et al., 2016; Kienast et al., 2001; Koutavas et al., 2002; Koutavas & Sachs, 2008; Lea et al., 2000, 2006; Leduc et al., 2007; Rosenthal et al., 2003; Stott et al., 2007). This suggests the EPWP and western equatorial Pacific warm pool primarily respond to pCO_2-radiative forcing (and associated feedbacks), while the cold tongue responds to pCO_2-radiative and dynamic forcing. This dynamic forcing includes a deep thermocline, which limited the ability of Ekman pumping to bring cold water to the surface and further cool the cold tongue.

A deep EEP thermocline could have reduced ENSO variability during the LGM by weakening the thermocline feedback that initiates and propagates ENSO (Ford et al., 2015; Manucharyan & Fedorov, 2014; Zhu et al., 2017). Reconstructions based on single foraminifera analyses show either reduced (Ford et al., 2015; Leduc et al., 2009) or enhanced (Koutavas & Joanides, 2012; Sadekov et al., 2013) ENSO during the LGM. Additional ENSO variability reconstructions are needed to reconcile these records (Lu et al., 2018). Much of the disagreement may depend on site location and choice of foraminifera species (Ford et al., 2015; Thirumalai et al., 2013). Studies aiming to reconstruct ENSO variability should carefully select sites that are sensitive to changes in ENSO (and not the seasonal cycle; Thirumalai et al., 2013) and preferably use surface-dwelling foraminifera (Ford et al., 2015). Using thermocline dwelling foraminifera to reconstruct ENSO variability is difficult due to changes in mean thermocline depth and possible foraminifera calcification depth preferences (this study; Ford et al., 2015; Zhu et al., 2017). If thermocline dwelling foraminifera are used, reconstructing the $\delta^{18}O$ depth profile using our Monte Carlo approach may deconvolve variability changes related to thermocline depth and ENSO variability. Understanding changes in thermocline depth is important to isolating the ENSO feedback mechanisms important to different mean climate states (Manucharyan & Fedorov, 2014).

4. Conclusions

During the LGM, the EEP thermocline was weaker and deeper in the EPWP and cold tongue region than during the Holocene. We use the $\delta^{18}O$ values of multiple species of foraminifera at Site 849 along with new and existing records of surface and subsurface $\delta^{18}O$ to show that the subsurface-to-surface $\delta^{18}O$ gradient was reduced during the LGM. This deep thermocline contributed to reduced productivity throughout the region and unequal temperature change between the EPWP and cold tongue region during the LGM relative to the Holocene. The LGM was characterized by an El Niño-like mean state that included a reduced zonal SST gradient and a deep thermocline, which may have impacted ENSO variability.

Acknowledgments
We thank Wei Huang (LDEO) and John Robbins (TAMU) for laboratory assistance, Pratigya Polissar for data acquisition, and Kaustubh Thirumalai for his MATLAB® map script. Funding was provided by NSF OCE-1436014 (H. L. F.), NERC NE/N015045/1 (H.L.F.), and AGS-1502889 (J. F. M.). C. L. M. was supported by the LDEO REU Program NSF OCE-1359194 and U.S. Science Support Program IODP NSF OCE-1450528. We thank three anonymous reviewers whose comments improved the quality of our work and remember Robert Thunell for his research legacy. Original and published data can be found at https://www.ncdc.noaa.gov/paleo-search/ and https://doi.pangaea.de/10.1594/PANGAEA.884659. We thank the researchers who made their data accessible online.

References

Andreasen, D. H., & Ravelo, A. C. (1997). Tropical Pacific Ocean thermocline depth reconstructions for the Last Glacial Maximum. *Paleoceanography*, *12*(3), 395–413. https://doi.org/10.1029/97PA00822

Bé, A., Bishop, J., & Sverdlove, M. S. (1985). Standing stock, vertical distribution and flux of planktonic foraminifera in the Panama Basin. *Marine Micropaleontology*, *9*(4), 307–333. https://doi.org/10.1016/0377-8398(85)90002-7

Bemis, B., Spero, H., Bijma, J., & Lea, D. W. (1998). Reevaluation of the oxygen isotopic composition of planktonic foraminifera: Experimental results and revised paleotemperature equations. *Paleoceanography*, *13*(2), 150–160. https://doi.org/10.1029/98PA00070

Benway, H. M., Mix, A. C., Haley, B. A., & Klinkhammer, G. P. (2006). Eastern Pacific Warm Pool paleosalinity and climate variability: 0-30 kyr. *Paleoceanography*, *21*, PA3008. https://doi.org/10.1029/2005PA001208

Bradtmiller, L. I., Anderson, R. F., Fleisher, M. Q., & Burckle, L. H. (2006). Diatom productivity in the equatorial Pacific Ocean from the last glacial period to the present: A test of the silicic acid leakage hypothesis. *Paleoceanography*, *21*, PA4201. https://doi.org/10.1029/2006PA001282

Clark, P. U., Dyke, A. S., Shakun, J. D., Carlson, A. E., Clark, J., Wohlfarth, B., et al. (2009). The Last Glacial Maximum. *Science*, *325*(5941), 710–714. https://doi.org/10.1126/science.1172873

Costa, K. M., Jacobel, A. W., McManus, J. F., Anderson, R. F., Winckler, G., & Thiagarajan, N. (2017). Productivity patterns in the equatorial Pacific over the last 30,000 years. *Global Biogeochemical Cycles*, *31*, 850–865. https://doi.org/10.1002/2016GB005579

Costa, K. M., McManus, J. F., Anderson, R. F., Ren, H., Sigman, D. M., Winckler, G., et al. (2016). No iron fertilization in the equatorial Pacific Ocean during the last ice age. *Nature*, *529*(7587), 519–522. https://doi.org/10.1038/nature16453

Curry, W., Thunell, R., & Honjo, S. (1983). Seasonal-changes in the isotopic composition of planktonic-foraminifera collected in Panama Basin sediment traps. *Earth and Planetary Science Letters*, *64*(1), 33–43. https://doi.org/10.1016/0012-821X(83)90050-X

de Garidel-Thoron, T., Rosenthal, Y., Beaufort, L., Bard, E., Sonzogni, C., & Mix, A. C. (2007). A multiproxy assessment of the western equatorial Pacific hydrography during the last 30 kyr. *Paleoceanography*, *22*, PA3204. https://doi.org/10.1029/2006PA001269

Dubois, N., Kienast, M., Normandeau, C., & Herbert, T. D. (2009). Eastern equatorial Pacific cold tongue during the Last Glacial Maximum as seen from alkenone paleothermometry. *Paleoceanography*, *24*, PA4207. https://doi.org/10.1029/2009PA001781

Fairbanks, R. G. (1989). A 17, 000-year glacio-eustatic sea level record: Influence of glacial melting rates on the younger Dryas event and deep-ocean circulation. *Nature*, *342*(6250), 637–642. https://doi.org/10.1038/342637a0

Fairbanks, R. G., Sverdlove, M., Free, R., Wiebe, P. H., & Bé, A. W. (1982). Vertical distribution and isotopic fractionation of living planktonic foraminifera from the Panama Basin. *Nature*, *298*(5877), 841–844. https://doi.org/10.1038/298841a0

Fan, W., Jian, Z., Chu, Z., Dang, H., Wang, Y., Bassinot, F., et al. (2018). Variability of the Indonesian throughflow in the Makassar Strait over the last 30 ka. *Scientific Reports*, *8*(1), 1–8. https://doi.org/10.1038/s41598-018-24055-1

Faul, K., Ravelo, A. C., & Delaney, M. (2000). Reconstructions of upwelling productivity, and photic zone depth in the eastern equatorial Pacific Ocean using planktonic foraminiferal stable isotopes and abundances. *Journal of Foraminiferal Research*, *30*(2), 110–125. https://doi.org/10.2113/0300110

Fiedler, P., & Talley, L. (2006). Hydrography of the eastern tropical Pacific: A review. *Progress in Oceanography*, *69*(2–4), 143–180. https://doi.org/10.1016/j.pocean.2006.03.008

Ford, H. L., Ravelo, A. C., & Polissar, P. J. (2015). Reduced El Niño–Southern Oscillation during the Last Glacial Maximum. *Science*, *347*(6219), 255–258. https://doi.org/10.1126/science.1258437

Guilyardi, E., Wittenberg, A., Fedorov, A., Collins, M., Wang, C., Capotondi, A., et al. (2009). Understanding El Niño in ocean–atmosphere general circulation models: Progress and challenges. *Bulletin of the American Meteorological Society*, *90*(3), 325–340. https://doi.org/10.1175/2008BAMS2387.1

Hertzberg, J. E., Schmidt, M. W., Bianchi, T. S., Smith, R. W., Shields, M. R., & Marcantonio, F. (2016). Comparison of eastern tropical Pacific TEX86 and Globigerinoides ruber Mg/Ca derived sea surface temperatures: Insights from the Holocene and Last Glacial Maximum. *Earth and Planetary Science Letters*, *434*(C), 320–332. https://doi.org/10.1016/j.epsl.2015.11.050

Hollstein, M., Mohtadi, M., Rosenthal, Y., Moffa-Sanchez, P., Oppo, D., Martínez Méndez, G., et al. (2017). Stable oxygen isotopes and Mg/Ca in Planktic foraminifera from modern surface sediments of the Western Pacific Warm Pool: Implications for thermocline reconstructions. *Paleoceanography*, *32*, 1174–1194. https://doi.org/10.1002/2017PA003122

Jakob, K. A., Pross, J., Scholz, C., Fiebig, J., & Friedrich, O. (2017). Thermocline state change in the eastern equatorial Pacific during the late Pliocene/early Pleistocene intensification of northern hemisphere glaciation. *Climate of the Past Discussions*, 1–22. https://doi.org/10.5194/cp-2017-151

Kawahata, H., Nishimura, A., & Gagan, M. K. (2002). Seasonal change in foraminiferal production in the western equatorial Pacific Warm Pool: Evidence from sediment trap experiments. *Deep-Sea Research Part II*, *49*(13–14), 2783–2800. https://doi.org/10.1016/S0967-0645(02)00058-9

Kienast, M., Steinke, S., Stattegger, K., & Calvert, S. (2001). Synchronous tropical South China Sea SST change and Greenland warming during deglaciation. *Science*, *291*(5511), 2132–2134. https://doi.org/10.1126/science.1057131

Koutavas, A., & Joanides, S. (2012). El Niño–Southern Oscillation extrema in the Holocene and Last Glacial Maximum. *Paleoceanography*, *27*, PA4208. https://doi.org/10.1029/2012PA002378

Koutavas, A., & Lynch-Stieglitz, J. (2003). Glacial-interglacial dynamics of the eastern equatorial Pacific cold tongue-intertropical convergence zone system reconstructed from oxygen isotope records. *Paleoceanography*, *18*(4), 1089. https://doi.org/10.1029/2003PA000894

Koutavas, A., Lynch-Stieglitz, J., Marchitto, T. M. Jr., & Sachs, J. P. (2002). El Nino-like pattern in ice age tropical Pacific sea surface temperature. *Science*, *297*(5579), 226–230. https://doi.org/10.1126/science.1072376

Koutavas, A., & Sachs, J. P. (2008). Northern timing of deglaciation in the eastern equatorial Pacific from alkenone paleothermometry. *Paleoceanography*, *23*, PA4205. https://doi.org/10.1029/2008PA001593

Lea, D. W., Pak, D. K., Belanger, C. L., Spero, H. J., Hall, M. A., & Shackleton, N. J. (2006). Paleoclimate history of Galapagos surface waters over the last 135,000 yr. *Quaternary Science Reviews*, *25*(11-12), 1152–1167. https://doi.org/10.1016/j.quascirev.2005.11.010

Lea, D. W., Pak, D. K., & Spero, H. J. (2000). Climate impact of late Quaternary equatorial Pacific sea surface temperature variations. *Science*, *289*(5485), 1719–1724. https://doi.org/10.1126/science.289.5485.1719

Leduc, G., Vidal, L., Cartapanis, O., & Bard, E. (2009). Modes of eastern equatorial Pacific thermocline variability: Implications for ENSO dynamics over the last glacial period. *Paleoceanography*, *24*, PA3202. https://doi.org/10.1029/2008PA001701

Leduc, G., Vidal, L., Tachikawa, K., Rostek, F., Sonzogni, C., Beaufort, L., & Bard, E. (2007). Moisture transport across Central America as a positive feedback on abrupt climatic changes. *Nature*, *445*(7130), 908–911. https://doi.org/10.1038/nature05578

Legrande, A. N., & Schmidt, G. A. (2006). Global gridded data set of the oxygen isotopic composition in seawater. *Geophysical Research Letters*, *33*, L12604. https://doi.org/10.1029/2006GL026011

Locarnini, A. R., Mishonov, A. V., Antonov, J. I., Boyer, T. P., Garcia, H. E., Baranova, O. K., et al. (2010). In S. Levitus (Ed.), *World ocean atlas 2009, volume 1: Temperature*. Washington, DC: NOAA Atlas NESDIS 68, U.S. Government Printing Office.

Loubere, P. (2000). Marine control of biological production in the eastern equatorial Pacific Ocean. *Nature*, *406*(6795), 497–500. https://doi.org/10.1038/35020041

Loubere, P. (2001). Nutrient and oceanographic changes in the eastern equatorial Pacific from the last full glacial to the present. *Global and Planetary Change*, *29*(1-2), 77–98. https://doi.org/10.1016/S0921-8181(00)00085-0

Loveley, M. R., Marcantonio, F., Wisler, M. M., Hertzberg, J. E., Schmidt, M. W., & Lyle, M. (2017). Millennial-scale iron fertilization of the eastern equatorial Pacific over the past 100,000 years. *Nature Geoscience*, *10*(10), 760–764. https://doi.org/10.1038/ngeo3024

Lu, Z., Liu, Z., Zhu, J., & Cobb, K. M. (2018). A review of paleo El Niño-Southern Oscillation. *Atmosphere*, *9*(4), 130–127. https://doi.org/10.3390/atmos9040130

Lyle, M., Mix, A., & Pisias, N. (2002). Patterns of CaCO 3deposition in the eastern tropical Pacific Ocean for the last 150 kyr: Evidence for a southeast Pacific depositional spike during marine isotope stage (MIS) 2. *Paleoceanography*, *17*(2), 1013. https://doi.org/10.1029/2000PA000538

Lyle, M., Murray, D. W., Finney, B. P., Dymond, J., Robbins, J. M., & Brooksforce, K. (1988). The record of Late Pleistocene biogenic sedimentation in the eastern tropical Pacific Ocean. *Paleoceanography*, *3*(1), 39–59. https://doi.org/10.1029/PA003i001p00039

Lynch-Stieglitz, J., Polissar, P. J., Jacobel, A. W., Hovan, S. A., Pockalny, R. A., Lyle, M., et al. (2015). Glacial-interglacial changes in central tropical Pacific surface seawater property gradients. *Paleoceanography*, *30*, 423–438. https://doi.org/10.1002/2014PA002746

Manucharyan, G. E., & Fedorov, A. V. (2014). Robust ENSO across a wide range of climates. *Journal of Climate*, *27*(15), 5836–5850. https://doi.org/10.1175/JCLI-D-13-00759.1

Martínez, I., Keigwin, L., Barrows, T. T., Yokoyama, Y., & Southon, J. (2003). La Niña-like conditions in the eastern equatorial Pacific and a stronger Choco jet in the northern Andes during the last glaciation. *Paleoceanography*, *18*(2), 1033. https://doi.org/10.1029/2002PA000877

Matsui, H., Nishi, H., Kuroyanagi, A., Hayashi, H., Ikehara, M., & Takashima, R. (2017). Vertical thermal gradient history in the eastern equatorial Pacific during the early to middle Miocene: Implications for the equatorial thermocline development. *Paleoceanography*, *32*, 729–743. https://doi.org/10.1002/2016PA003058

Mix, A., Pisias, N., Rugh, W., Wilson, J., Morey, A., & Hagelberg, T. (1995). 17. Benthic foraminifer stable isotope record from site 849 (0-5Ma): Local and global climate changes. *Proceeding of the Ocean Drilling Program, Scientific Results*, *138*, 371–412.

Murray, R. W., Leinen, M., & Knowlton, C. W. (2012). Links between iron input and opal deposition in the Pleistocene equatorial Pacific Ocean. *Nature Geoscience*, *5*(4), 270–274. https://doi.org/10.1038/ngeo1422

Nathan, S., & Leckie, R. (2009). Early history of the Western Pacific Warm Pool during the middle to late Miocene (~ 13.2–5.8 Ma): Role of sea-level change and implications for equatorial circulation. *Palaeogeogr Palaeocl*, *274*(3-4), 140–159. https://doi.org/10.1016/j.palaeo.2009.01.007

Otto-Bliesner, B. L., Schneider, R., Brady, E. C., Kucera, M., Abe-Ouchi, A., Bard, E., et al. (2009). A comparison of PMIP2 model simulations and the MARGO proxy reconstruction for tropical sea surface temperatures at Last Glacial Maximum. *Climate Dynamics*, *32*(6), 799–815. https://doi.org/10.1007/s00382-008-0509-0

Patrick, A., & Thunell, R. (1997). Tropical Pacific sea surface temperatures and upper water column thermal structure during the Last Glacial Maximum. *Paleoceanography*, *12*(5), 649–657. https://doi.org/10.1029/97PA01553

Pena, L. D., Cacho, I., Ferretti, P., & Hall, M. A. (2008). El Nino-Southern Oscillation-like variability during glacial terminations and interlatitudinal teleconnections. *Paleoceanography*, *23*, PA3101. https://doi.org/10.1029/2008PA001620

Pena, L. D., Goldstein, S. L., Hemming, S. R., Jones, K. M., Calvo, E., Pelejero, C., & Cacho, I. (2013). Rapid changes in meridional advection of Southern Ocean intermediate waters to the tropical Pacific during the last 30 kyr. *Earth and Planetary Science Letters*, *368*(C), 20–32. https://doi.org/10.1016/j.epsl.2013.02.028

Pichat, S., Sims, K. W. W., Francois, R., McManus, J. F., Brown Leger, S., & Albarède, F. (2004). Lower export production during glacial periods in the equatorial Pacific derived from (231Pa/230Th) xs, 0 measurements in deep-sea sediments. *Paleoceanography*, *19*, PA4023. https://doi.org/10.1029/2003PA000994

Pichevin, L. E., Reynolds, B. C., Ganeshram, R. S., Cacho, I., Pena, L., Keefe, K., & Ellam, R. M. (2009). Enhanced carbon pump inferred from relaxation of nutrient limitation in the glacial ocean. *Nature*, *459*(7250), 1114–1117. https://doi.org/10.1038/nature08101

Rafter, P. A., Sigman, D. M., Charles, C. D., Kaiser, J., & Haug, G. H. (2012). Subsurface tropical Pacific nitrogen isotopic composition of nitrate: Biogeochemical signals and their transport. *Global Biogeochemical Cycles*, *26*, GB1003. https://doi.org/10.1029/2010GB003979

Ravelo, A. C., & Fairbanks, R. G. (1992). Oxygen isotopic composition of multiple species of planktonic foraminifera: Recorders of the modern photic zone temperature gradient. *Paleoceanography*, *7*(6), 815–831. https://doi.org/10.1029/92PA02092

Ravelo, A. C., & Shackleton, N. J. (1995). Evidence for surface-water circulation changes at site 851 in the eastern tropical Pacific Ocean. *Proceeding of the Ocean Drilling Program, Scientific Results*, *138*, 503–514. https://doi.org/10.2973/odp.proc.sr.138.126.1995

Rebert, J. P., Donguy, J. R., Eldin, G., & Wyrtki, K. (1985). Relations between sea level, thermocline depth, heat content, and dynamic height in the tropical Pacific Ocean. *Journal of Geophysical Research*, *90*(C6), 11,719–11,725. https://doi.org/10.1029/JC090iC06p11719

Rebotim, A., Voelker, A. H. L., Jonkers, L., Waniek, J. J., Meggers, H., Schiebel, R., et al. (2016). Factors controlling the depth habitat of planktonic foraminifera in the subtropical eastern North Atlantic. *Biogeosciences Discussions*, 1–48. https://doi.org/10.5194/bg-2016-348

Richards, K. J., & Pollard, R. T. (1991). Structure of the upper ocean in the western equatorial Pacific. *Nature*, *350*(6313), 48–50. https://doi.org/10.1038/350048a0

Rincón-Martínez, D., Steph, S., Lamy, F., Mix, A., & Tiedemann, R. (2011). Tracking the equatorial front in the eastern equatorial Pacific Ocean by the isotopic and faunal composition of planktonic foraminifera. *Marine Micropaleontology*, *79*(1–2), 24–40. https://doi.org/10.1016/j.marmicro.2011.01.001

Rosenthal, Y., Oppo, D., & Linsley, B. K. (2003). The amplitude and phasing of climate change during the last deglaciation in the Sulu Sea, western equatorial Pacific. *Geophysical Research Letters*, *30*(8), 1428. https://doi.org/10.1029/2002GL016612

Sadekov, A. Y., Ganeshram, R., Pichevin, L., Berdin, R., McClymont, E. L., Elderfield, H., & Tudhope, A. W. (2013). Palaeoclimate reconstructions reveal a strong link between El Nino-Southern Oscillation and tropical Pacific mean state. *Nature Communications*, *4*(1), 1–8. https://doi.org/10.1038/ncomms3692

Sagawa, T., Yokoyama, Y., Ikehara, M., & Kuwae, M. (2011). Vertical thermal structure history in the western subtropical North Pacific since the Last Glacial Maximum. *Geophysical Research Letters*, *38*, L00F02. https://doi.org/10.1029/2010GL045827

Sarmiento, J. L., Gruber, N., Brzezinski, M. A., & Dunne, J. P. (2004). High-latitude controls of thermocline nutrients and low latitude biological productivity. *Nature*, *427*(6969), 56–60. https://doi.org/10.1038/nature02127

Spero, H., Mielke, K., Kalve, E., Lea, D. W., & Pak, D. (2003). Multispecies approach to reconstructing eastern equatorial Pacific thermocline hydrography during the past 360 kyr. *Paleoceanography*, *18*(1), 1022. https://doi.org/10.1029/2002PA000814

Spero, H. J., & Lea, D. W. (2002). The cause of carbon isotope minimum events on glacial terminations. *Science*, *296*(5567), 522–525. https://doi.org/10.1126/science.1069401

Stott, L., Timmermann, A., & Thunell, R. (2007). Southern hemisphere and deep-sea warming led deglacial atmospheric CO_2 rise and tropical warming. *Science*, *318*(5849), 435–438. https://doi.org/10.1126/science.1143791

Thirumalai, K., Partin, J. W., Jackson, C. S., & Quinn, T. M. (2013). Statistical constraints on El Niño Southern Oscillation reconstructions using individual foraminifera: A sensitivity analysis. *Paleoceanography*, *28*, 401–412. https://doi.org/10.1002/palo.20037

Thunell, R. C., Curry, W. B., & Honjo, S. (1983). Seasonal variation in the flux of planktonic foraminifera: Time series sediment trap results from the Panama Basin. *Earth and Planetary Science Letters*, *64*(1), 44–55. https://doi.org/10.1016/0012-821X(83)90051-1

Venancio, I. M., Belem, A. L., Santos, T. P., Lessa, D. O., Albuquerque, A. L. S., Mulitza, S., et al. (2017). Calcification depths of planktonic foraminifera from the southwestern Atlantic derived from oxygen isotope analyses of sediment trap material. *Marine Micropaleontology*, *136*, 37–50. https://doi.org/10.1016/j.marmicro.2017.08.006

Watkins, J. M., Mix, A. C., & Wilson, J. (1996). Living planktic foraminifera: Tracers of circulation and productivity regimes in the central equatorial Pacific. *Deep-Sea Research Part II*, *43*(4-6), 1257–1282. https://doi.org/10.1016/0967-0645(96)00008-2

Wyrtki, K. (1981). An estimate of equatorial upwelling in the Pacific. *Journal of Physical Oceanography*, *11*(9), 1205–1214. https://doi.org/10.1175/1520-0485(1981)011<1205:AEOEUI>2.0.CO;2

Xu, J., Kuhnt, W., Holbourn, A., Regenberg, M., & Andersen, N. (2010). Indo-Pacific Warm Pool variability during the Holocene and Last Glacial Maximum. *Paleoceanography*, *25*, PA4230. https://doi.org/10.1029/2010PA001934

Zhu, J., Liu, Z., Brady, E., Otto-Bliesner, B., Zhang, J., Noone, D., et al. (2017). Reduced ENSO variability at the LGM revealed by an isotope-enabled Earth system model. *Geophysical Research Letters*, *44*, 6984–6992. https://doi.org/10.1002/2017GL073406